INSTITUTE OF PHYSICS PUBLISHING NANOTECHNOLOGY
Nanotechnology **17** (2006) 2590–2594 doi:10.1088/0957-4484/17/10/024

Integration of single-crystalline nanocolumns into highly ordered nanopore arrays

G Q Ding, W Z Shen[1], M J Zheng and Z B Zhou

Laboratory of Condensed Matter Spectroscopy and Opto-Electronic Physics, Department of Physics, Shanghai Jiao Tong University, 1954 Hua Shan Road, Shanghai 200030, People's Republic of China

E-mail: wzshen@sjtu.edu.cn

Received 1 February 2006
Published 28 April 2006
Online at stacks.iop.org/Nano/17/2590

Abstract
The arrangement of nanostructures into desired well-ordered architectures is crucial for the realization of functional nanodevices and has been the focus of current nanotechnology. Existing physical and chemical approaches have the ability to assemble nanostructures, but it is still a challenge to arrange basic nanostructures into a highly ordered designed pattern. Here, we report a novel method to integrate tin-doped indium oxide single-crystalline nanocolumns into highly ordered two-dimensional nanopore patterns through radio-frequency magnetron sputtering by the aid of porous alumina membranes (PAMs). We have further demonstrated that the morphology of the assembled nanopore arrays is controllable by adjusting either the PAM configurations or sputtering conditions. Our present method provides the possibility of a general approach for nanounit integration, and these assembled regular nanopore arrays pave the way for the application of novel filters and sensors.

1. Introduction

Many kinds of basic nanostructure units, such as nanoparticles, nanodots, nanorods, nanowires, nanobelts and nanotubes, have been synthesized under various methods. However, the assembly or integration of these nanostructures into desired well-ordered architectures is crucial for the realization of functional nanodevices and has been the focus of current nanotechnology [1]. The assembly strategies can be classified into two main categories, i.e., the physical and chemical approaches. The physical methods include electric/magnetic field alignment [2], precisely epitaxial growth [3, 4], multistep vapour–liquid–solid growth mode [5, 6], and nanolithographic techniques [7], etc. Generally, the physical approaches are time-consuming and complex, although large-scale samples with specific patterns can be obtained. On the other hand, the chemical methods mainly rely on the electrostatic attraction between opposite charges in chemical solution, e.g., polyelectrolytes' adsorption of ions [8], strong coordination interactions of biomolecules (DNA, proteins, etc) with other charged basic nanostructures [9–11], and colloidal aggregation [12, 13]. Most of the chemical approaches are based on suspensions, incurring all the contamination problems of wet processing. Extra steps are needed to integrate the chemically assembled nanostructures onto solid substrates by employing, e.g., the Langmuir–Blodgett [14] and surface chemistry modification [15] techniques.

This paper reports a simple one-step physical approach to assemble nanocolumns into highly ordered two-dimensional (2D) nanopore patterns through radio-frequency (RF) magnetron sputtering by the aid of porous alumina membranes (PAMs). The demonstration of this integration method has been carried out on tin-doped indium oxide (ITO). As we know, indium oxide (In_2O_3) has a direct bandgap of ∼3.6 eV and has been widely used in solar cells, organic light emitting diodes, gas sensors, and windows that absorb sunlight [16–18]. In_2O_3 can also be one of the most attractive conductive oxides for field emission because of its convenience of n-type doping, relatively low electron affinity, high chemical inert-

[1] Author to whom any correspondence should be addressed.

 © 2006 IOP Publishing Ltd Printed in the UK

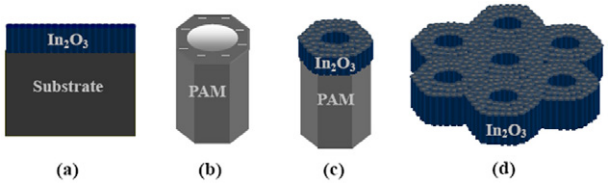

Figure 1. Schematic diagrams of (a) ITO nanocolumns grown on Si substrates, (b) a single cell of hexagonal PAM with localized negative charges at the top surface, (c) ITO sputtered on top of PAM copying the morphology of the PAM's nanopore, (d) highly ordered hexagonal ITO nanopore array.

(This figure is in colour only in the electronic version)

ness, and sputter resistance. As a result, many kinds of In_2O_3 nanostructures have been fabricated recently, including nanoparticles [19, 20], nanowires [21, 22], nanochains [23], nanofibres [24], nanobelts [25], nanotubes [26] and nanopyramids [27]. The present successful realization of 2D nanopores will not only provide a novel assembly method, but also further improve performances and broaden applications of In_2O_3.

The basic idea of assembling ITO nanocolumns into 2D nanopores comes from the unique properties of both the sputtering technique and PAMs. Due to controllable adatom mobility and different growth rates along various directions, many kinds of nanoscale microstructures can be synthesized under the magnetron sputtering. The three-zone model, proposed by Movchan and Demchishin [28] and later developed by Thornton [29], can describe well the sputtered microstructures with columnar, tapered, and fibrous grains. Metal [28] (such as Ni, Ti, and W) and oxide (such as Al_2O_3 [28], ZrO_2 [28], ZnO [30], MgO [31], and In_2O_3 [32]) nanocolumns have been realized under appropriate argon pressures and T/T_m values (where T is the substrate temperature and T_m is the material melting point). Therefore, as shown in figure 1(a), ITO thin films with a nanocolumn microstructure can be grown on different substrates. On the other hand, PAMs are versatile templates, which have circle nanopores and hexagonal cells with controllable pore diameter, interpore spacing, and thickness [33, 34]. Figure 1(b) displays schematically a single cell of PAM with negative charges localized at the intermediate part of its top surface due to the inhomogeneous distribution of anion species ($C_2O_4^{2-}$ and OH^-) [35, 36]. During the deposition of sputtered ITO on PAMs with, e.g., Si substrates, these localized negative charges can attract ions, resulting in ITO nucleation and growth along the preferable directions at the PAM top surfaces. Due to the easy arrangement of columns, ITO nanocolumns can be assembled to form a hexagonal cell pattern identical to that of the PAMs, as shown schematically in figure 1(c). We therefore expect that well-ordered and large-scale ITO nanopore arrays (see figure 1(d)) can be fabricated on the top surfaces of the PAMs.

2. Experimental details

To realize the above proposal, we first prepare ultrathin PAMs with different pore diameters and thicknesses through a typical two-step anodizing procedure [33], then transfer free-standing PAMs onto Si(100) substrates [34], and finally dry the whole specimen for the sputtering of ITO. PAMs with the pore diameter of 30–90 nm and interpore spacing of 100 nm were fabricated through a typical two-step anodizing procedure with aluminium foil as the anode in 0.1 M oxalic acid electrolyte [33, 34]. The unoxided aluminium was removed in a saturated $CuSO_4$-based solution and, throughout, free-standing PAMs with controllable pore diameters were obtained by dissolving the barrier layers in phosphoric acid for different times [34]. PAMs with the large pore diameter of ∼170 nm and interpore spacing of ∼350 nm were fabricated by anodizing Al foil in 0.5 M phosphoric acid under 140 V and 0 °C through the same two-step anodizing procedure. A parallel-plate RF magnetron sputtering system with a power of 60 W and frequency of 13.56 MHz was used to grow ITO layers. The ITO sputtering target was hot-pressed oxide ceramic (90 wt% ITO and 10 wt% SnO_2 with purity of 99.99%), and the sputtering gas was 99.999% argon. The working chamber was pumped lower than 1×10^{-3} Pa before sputtering, and the space between target and substrate was fixed at a short distance of 2.6 cm. The substrate was heated to 180 °C before deposition and, during sputtering, the substrate temperature was also kept at 180 °C and the argon pressure was 0.5 Pa with a deposition rate of ∼3 nm min^{-1}. After sputtering, the specimen was naturally cooled to room temperature in the chamber.

3. Results and discussion

The evidence for the nanocolumn growth of the sputtered ITO can be observed directly in high-magnification field-emission scanning electron microscope (FE-SEM by Philips XL30FEG) images. The top view image (figure 2(a)) clearly demonstrates that the sputtered ITO has many nanopores surrounded by nanoscale grains with a size of ∼15 nm on the surface. The as-prepared specimens were cut to observe the cross section of ITO nanopores on top of the PAM under FE-SEM (figure 2(b)), which reveals that these grains have a nanocolumn microstructure with a height of ∼50 nm. The nanocolumn nature of ITO grains can be further confirmed by high-resolution transmission electron microscope (HRTEM by JEOL JEM-2100F) images of both the top surface (figure 2(c)) and the side view (figure 2(d)), where good arrangement of the nanocolumns and interfaces of the ITO grains can be observed clearly, and the size, shape and arrangement of these sputtered ITO nanocolumns are consistent with the FE-SEM observations. During HRTEM measurements, the ITO layer was removed from the PAM by dissolving the PAM layer in diluted alkaline solution and transferred onto the copper grid to observe the top surface of the ITO nanopores, while, for the observation of the side surface, the free-standing ITO nanopores were ground and dispersed onto a copper grid.

It is interesting to note that the top surface of a single ITO nanocolumn displays pyramid-like morphology with ∼5 nm high triangular facets (see figures 2(b) and (d)). The small facets can be indexed to the In_2O_3(222) planes with clear interplanar spacing of 0.290 nm through the HRTEM image of figure 2(e). The formation of triangular facets is due to the fact that, during the crystal growth of In_2O_3, the (222) plane with slower growth rate tends to appear as facets over the fast-growing plane, which has been demonstrated in the synthesis of In_2O_3 nanopyramids [27]. The atomic-resolution HRTEM

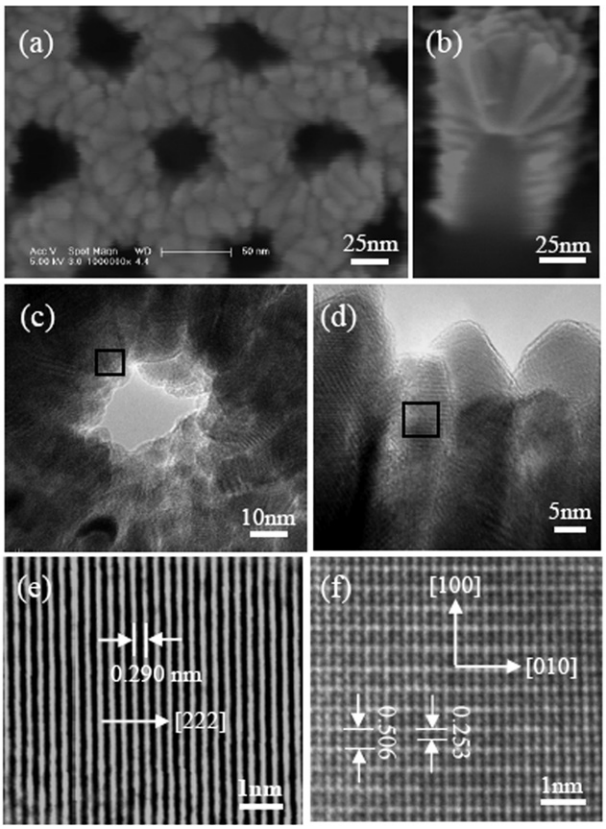

Figure 2. (a) Top and (b) cross-sectional view FE-SEM images of ITO on top of the PAM; (c) HRTEM image of a single ITO nanopore; (d) HRTEM image shows several well-arranged ITO nanocolumns; (e) top surface HRTEM image from the box in (c) reveals that the (222) fringes are separated by 0.290 nm; (f) side surface HRTEM image from the box in (d) demonstrates the growth orientation along the nanocolumns of [100].

image (figure 2(f)) of a single nanocolumn's side surface clearly reveals the lattice distances of both 0.506 nm for plane (200) and 0.253 nm for plane (400). These HRTEM results confirm that every ITO nanocolumn is single crystalline, and that the growth orientations perpendicular and parallel to the top surfaces of PAMs are [100] and [010], respectively, while the top surface of the nanocolumns is indexed to (222) planes. The growth along the [100] direction is much faster than that along the [222] direction, resulting in the column microstructure with pyramid-like top morphology. Such a preferable [100] growth orientation in the formation of ITO nanocolumns has also been observed in the reported In_2O_3 nanowires [21, 22], nanofibres [24], and nanobelts [25], with the different configurations being due to the various growth conditions.

The above arguments clearly demonstrate that we have successfully assembled the 2D ITO nanopores from well-arranged nanocolumns. In fact, benefitting from the large-scale fabrication of the PAMs [33], the synthesized samples have a surface area of over several square centimetres. Figure 3(a) displays the top view FE-SEM image of ITO nanopores on top of a PAM, which reveals the two-layer structure, i.e., the top ITO nanopore layer and the bottom PAM layer. The enlarged top view morphology of ITO nanopores (figure 3(b)) reveals a highly ordered hexagonal pattern with a pore size of ∼50 nm

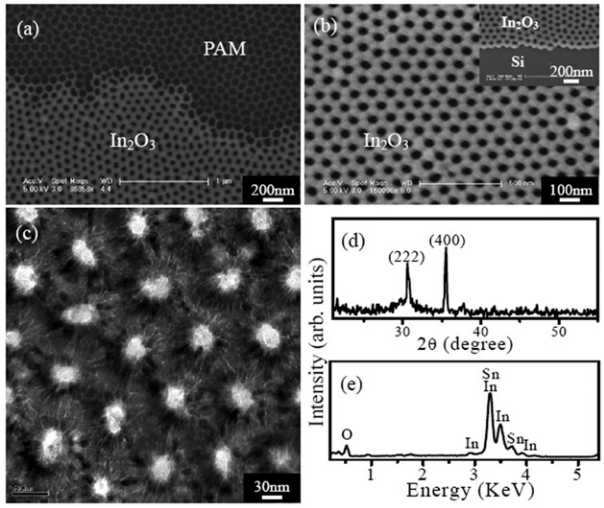

Figure 3. (a) FE-SEM image of the top surface morphology of a typical ITO nanopore array on top of a PAM; (b) FE-SEM image of the enlarged ITO nanopores, the inset is the FE-SEM image of the free-standing ITO nanopore arrays directly transferred onto a Si substrate; (c) TEM image, (d) XRD, and (e) EDX spectra of the ITO nanopores.

and interpore spacing of ∼100 nm, confirming that the 2D ITO nanopores basically copy the PAM surface morphology. It should be noted that nearly all of the ITO deposits on top of the PAM, which is totally different to the growth process of nanodot arrays using PAMs as templates [33]. What is more, the ITO nanopores can be taken from the PAM intact, and transferred onto different substrates, such as Si substrates, as shown in the inset in figure 3(b). HRTEM observation (figure 3(c)) can further confirm the assembly of ITO nanopores with regular interpore spacing and pore diameter, where the short white lines with a length of ∼10 nm are the interfaces of ITO nanocolumns. The successful assembly of highly ordered and large-scale 2D ITO nanopores is due to the electronic attraction between the localized charges in PAMs and the sputtered well-arranged ITO nanocolumns, as proposed in the schematic diagram of figure 1.

We have further characterized the microstructure of the obtained 2D nanopores with the aid of x-ray diffraction (XRD by Bruker D8 ADVANCE system) and energy dispersive spectroscopy (EDS). The two diffraction peaks in figure 3(d) can be attributed to the (222) and (400) planes of the cubic In_2O_3 structure of Mn_2O_3 (I) type, with a cell constant of 1.012 nm [32]. We note that the strongest diffraction peak of the ITO nanopores is (400), while in bulk In_2O_3 the strongest peak is (222) with a relative intensity of the (400) plane of 35 (JCPDF No. 44-1087). The XRD results coincide well with the above-demonstrated (222) facets and preferable [100] growth orientation of ITO nanocolumns through the HRTEM images. The EDS analysis during HRTEM observation (figure 3(e)) reveals that there are three elements in the nanopores, i.e., indium, tin and oxygen, with an approximate atomic ratio of indium to tin of 12:1. Both the XRD and EDS results confirm that the obtained nanopores are really composed of tin-doped In_2O_3. The resistivity of the ITO nanopores is only $\sim 4 \times 10^{-4}$ Ω cm, which is beneficial for the application of the highly ordered 2D ITO nanopores in nanoelectronic devices.

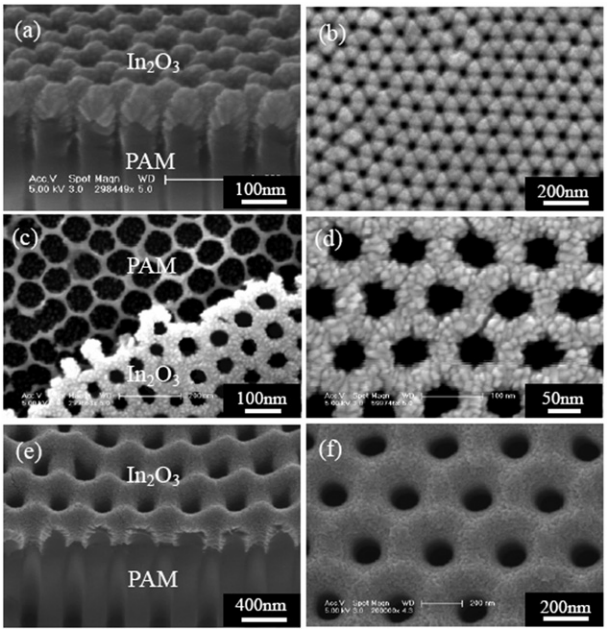

Figure 4. (a) Cross-sectional and (b) top view FE-SEM images of ITO nanopores on top of a PAM with a small pore diameter of ∼30 nm; (c) and (d) top views of ITO nanopores sputtered on a PAM with pore diameter of ∼90 nm; (e) cross-sectional and (f) top morphology of ITO nanopores on top of a PAM with a large pore diameter of ∼170 nm.

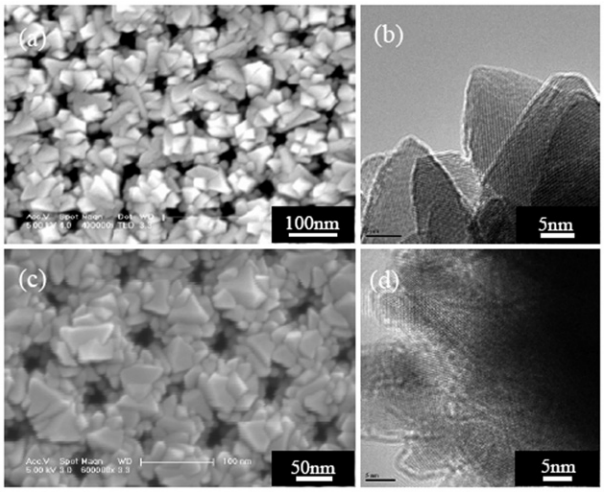

Figure 5. (a) Top view FE-SEM image of ITO nanopores sputtered on a PAM, and (b) HRTEM image of the side surface of the ITO grains grown at a temperature of 250 °C and argon pressure of 0.5 Pa; (c) top view FE-SEM image of ITO nanopores sputtered on a PAM, and (d) HRTEM image of the side surface of the ITO grains grown at a temperature of 180 °C and argon pressure of 1.0 Pa.

Since the origin of the 2D nanopore formation is due to the electronic attraction between the localized charges in PAMs and the sputtered ITO nanoscale microstructures, we can control the integration process by adjusting either the PAM configurations or sputtering conditions. PAMs with controllable pore diameter, interpore spacing, and thickness can be fabricated easily under different anodizing voltages and electrolytes [33]. Figure 4 presents the effect of PAM pore diameter and interpore spacing on the morphology of ITO nanopores synthesized under the same RF magnetron sputtering conditions. For a small PAM pore diameter of ∼30 nm and interpore spacing of ∼100 nm (40 V and 0.1 M oxalic acid), the cross-sectional FE-SEM image of figure 4(a) reveals clearly that the ITO nanopores are on top of the PAMs, and the top view (figure 4(b)) demonstrates the yielded highly ordered hexagonal ITO nanopores with a pore diameter of ∼25 nm and interpore spacing of ∼100 nm. When the PAM (40 V and 0.1 M oxalic acid) pore diameter is broadened to ∼90 nm in 5 wt% phosphoric acid for 60 min, as shown in figure 4(c), the ITO nanopore layer can still copy the morphology of the PAM with a large pore diameter (∼60 nm) (figure 4(d)). The narrow PAM sidewall (∼10 nm) restricts good arrangement of the attracted ITO nanocolumns, limiting the pore diameter of the yielded ITO nanopores.

With much larger pore diameters of PAMs (e.g., ∼170 nm with ∼350 nm interpore spacing under 140 V and 0.5 M phosphoric acid), further increases of ITO nanopore diameter (∼140 nm) and interpore spacing (∼350 nm) have also been realized (see figures 4(e) and (f)). Since nearly all of the ITO sputters on top of the PAM (see e.g., figures 4(a) and (e)), the effect of PAM thickness can be neglected in the assembly of ITO nanopores. Our high-magnification FE-SEM and HRTEM observations confirm that all of the above tunable ITO nanopores are assembled from nanocolumns. This is reasonable, since they are all synthesized under the same sputtering conditions. The controllable morphology of the ITO nanopores by PAM configuration demonstrates not only the origin of the present 2D nanopore formation, but also the feasibility of the novel nanostructure assembly method.

In addition to the PAM configurations, the sputtering conditions, especially the growth temperature and argon pressure, will also play key roles in the integration of 2D ITO nanopores. Figure 5(a) shows the surface morphology of the sputtered ITO layer under the same growth conditions as in figures 2 and 3, except that the substrate temperature is 250 °C. It is found that the deposited ITO microstructure transforms from nanocolumns into faceted grains under higher temperatures, and that the height of the triangular facets even reaches 20 nm, as shown in the HRTEM image of figure 5(b). Both the enhanced surface and bulk diffusion ability of sputtered species contribute to such a microstructure transformation, which is consistent with the three-zone model [30, 31]. The ITO-faceted grains with an average grain size of ∼25 nm are hard to arrange regularly on top of the PAM, compared with that of the ITO nanocolumns (see figure 2(d)). It is the large faceted grains and irregular arrangement that lead to the observed small and nonuniform 2D ITO nanopores in figure 5(a). In fact, low growth temperature is helpful for obtaining nanocolumns using the sputtering technique [30, 31], except for the poor crystallization of ITO under too low a temperature [37].

The argon pressure is usually kept in the range 0.3–5.0 Pa while sputtering oxides [29–32]. High argon pressure will cause scattering of the energetic reflected species, which does harm to the preferable growth of the ITO nanocolumns. Figures 5(c) and (d) display the top view FE-SEM image of ITO nanopores and the HRTEM image of ITO grains sputtered at 180 °C and 1.0 Pa. It can be seen that some

nanopores are even clogged due to the scattering effect (figure 5(c)) and that the arrangement of the ITO grains is also not regular (figure 5(d)). Therefore, highly ordered 2D ITO nanopores should be assembled from the well-arranged nanocolumns, which requires optimal substrate temperature and argon pressure during magnetron sputtering.

4. Conclusions

In summary, we have proposed and realized a simple one-step approach for assembling single-crystalline tin-doped ITO nanocolumns into highly ordered and large-scale 2D nanopores through RF magnetron sputtering with the aid of versatile porous alumina membranes. Single-crystalline ITO nanocolumns were synthesized at an appropriate substrate temperature and argon pressure with the preferable [100] growth orientation. These easily arranged nanocolumns can be assembled into regular 2D nanopores through the electrostatic attraction of the localized charges in PAMs. We have further demonstrated that the morphology of the assembled ITO nanopores is controllable by adjusting either the PAM configuration (pore diameter and interpore spacing) or the sputtering conditions (substrate temperature and argon pressure), revealing that highly ordered 2D ITO nanopores should be assembled from the well-arranged nanocolumns.

It should be noted that the as-synthesized regular 2D ITO nanopores are assembled from nanocolumns at a significant percentage (near 100%) of yield without any other formation of ITO. The assembled regular ITO nanopores pave the way for the application of novel filters and sensors due to the large surface area and well-arranged nanocolumns. According to the proposal schematized in figure 1, it is clear that the present technique provides the possibility of fabricating nanopore arrays of other materials. For instance, we have also integrated ZnO grains into highly ordered nanopore arrays utilizing both the sputtering technology and a PAM template [38]. In addition, the crystalline semiconducting ITO nanopores have great advantages over amorphous PAMs, especially in the conductive and optical properties. Through epitaxial growth on the lattice planes, high-quality heterojunction nanostructures [3] can even be fabricated using ITO nanopores.

Acknowledgments

This work was supported by the Natural Science Foundation of China under contract Nos 10125416, 50572064, the Shanghai Major Projects of 03DJ14003, 05DJ14003, and the National Minister of Education Program for Changjiang Scholars and Innovative Research Team in University (PCSIRT).

References

[1] Friedman R S, Mcalpine M C, Ricketts D S, Ham D and Lieber C M 2005 *Nature* **434** 1085
[2] Hone J, Liaguno M C, Nemes N M, Johnson A T, Fischer J E, Walters D A, Casavant M J, Schmidt J and Smalley R E 2000 *Appl. Phys. Lett.* **77** 666
[3] Goldberger J, He R, Zhang Y F, Lee S, Yan H Q, Choi H J and Yang P D 2003 *Nature* **422** 599
[4] Wang X D, Summers C J and Wang Z L 2004 *Nano Lett.* **4** 423
[5] Dick K A, Deppert K, Larsson M W, Martensson T, Seifert W, Wallenberg L R and Samuelson L 2004 *Nat. Mater.* **3** 380
[6] Hu J Q, Bando Y S, Zhan J H, Yuan X L, Sekiguchi T and Golberg D 2005 *Adv. Mater.* **17** 971
[7] Wu Y, Xiang J, Yang C, Lu W and Lieber C M 2004 *Nature* **430** 61
[8] Minko S, Kiriy A, Gorodyska G and Stamm M 2002 *J. Am. Chem. Soc.* **124** 10192
[9] Keren K, Krueger M, Gilad R, Yoseph G B, Sivan U and Braun E 2002 *Science* **297** 72
[10] Warner M G and Hutchison J E 2003 *Nat. Mater.* **2** 272
[11] Becerril H A, Stoltenberg R M, Wheeler D R, Davis R C, Harb J N and Woolley A T 2005 *J. Am. Chem. Soc.* **127** 2828
[12] Kim M H, Im S K and Park O O 2005 *Adv. Funct. Mater.* **15** 1329
[13] Wang D and Möhwald H 2004 *Adv. Mater.* **16** 244
[14] Yang P D 2003 *Nature* **425** 243
[15] Myung S, Lee M, Kim G T, Ha J S and Hong S H 2005 *Adv. Mater.* **17** 2361
[16] Gutarra A, Azens A, Stjerna B and Granqvist C G 1994 *Appl. Phys. Lett.* **64** 1064
[17] Wu C C, Wu C I, Sturm J C and Kahn A 1997 *Appl. Phys. Lett.* **70** 1348
[18] Takada T, Suzukik K and Nakane M 1993 *Sensors Actuators* B **13** 404
[19] Seo W S, Jo H H, Lee K and Park J T 2003 *Adv. Mater.* **15** 795
[20] Murali A, Barve A, Leppert V J and Risbud S H 2001 *Nano Lett.* **1** 287
[21] Nguyen P, Ng H T, Kong J, Cassell A M, Quinn R, Li J, Han J, McNeil M and Meyyappan M 2003 *Nano Lett.* **3** 925
[22] Chun H J and Choi Y S 2004 *Appl. Phys. Lett.* **85** 461
[23] Lao J Y, Huang J Y, Wang D Z and Ren Z F 2004 *Adv. Mater.* **16** 65
[24] Liang C H, Meng G W, Lei Y, Phillipp F and Zhang L D 2001 *Adv. Mater.* **13** 1330
[25] Pan Z W, Dai Z R and Wang Z L 2001 *Science* **291** 1947
[26] Li Y B, Bando Y and Golberg D 2003 *Adv. Mater.* **15** 581
[27] Jia H B, Zhang Y, Chen X H, Shu J, Luo X H, Zhang Z S and Yu D P 2003 *Appl. Phys. Lett.* **82** 4146
[28] Movchan B A and Demchishin A V 1969 *Phys. Met. Metallogr.* **28** 653
[29] Thornton J A 1974 *J. Vac. Sci. Technol.* **11** 666
[30] Mirica E, Kowach G, Evans P and Du H 2004 *Cryst. Growth Des.* **4** 147
[31] Pinto P, Poothra J I, Purandare S C, Pai S P, D'Souza C P, Kumar D and Sharon M 1991 *J. Vac. Sci. Technol.* A **9** 2670
[32] Kulkarni A K, Schulz K H, Lim T S and Khan M 1997 *Thin Solid Film* **1** 308
[33] Chik H and Xu J M 2004 *Mater. Sci. Eng.* R **43** 103
[34] Ding G Q, Zheng M J, Xu W L and Shen W Z 2005 *Nanotechnology* **16** 1285
[35] Nielsch K, Choi J, Schwirn K, Wehrspon R B and Gösele U 2002 *Nano Lett.* **2** 677
[36] Choi J, Luo Y, Wehrspohn R B, Hillebrand R, Schilling J and Gösele U 2003 *J. Appl. Phys.* **94** 4757
[37] Hoshi Y and Kiyomura T 2002 *Thin Solid Films* **411** 36
[38] Ding G Q, Shen W Z, Zheng M J and Fan D H 2006 *Appl. Phys. Lett.* **88** 103106